From wood pulp fibers to tubular SiO_2/C composite as anode for Li-ion battery: in-situ regulation of cellulose microfibrils by alkali solution

Wang, Xiaodi; Liu, Xiuzhi; Ren, Xiaoli ; Luo, Kaisheng ; Xu, Wenyang; Hou, Qingxi ; Liu, Wei

Published in:
Industrial Crops and Products

DOI:
10.1016/j.indcrop.2020.113022

Published: 15/12/2020

Document Version
Accepted author manuscript

Document License
CC BY-NC-ND

From wood pulp fibers to tubular SiO_2/C composite as anode for Li-ion battery: in-situ regulation of cellulose microfibrils by alkali solution

Xiaodi Wang [a], Xiuzhi Liu [a], Xiaoli Ren [a], Kaisheng Luo [a], Wenyang Xu [c], Qingxi Hou [a,b]*, Wei Liu [a]*

[a] Tianjin Key Laboratory of Pulp and Paper, Tianjin University of Science & Technology, Tianjin 300457, China

[b] State Key Laboratory of Pulp and Paper Engineering, South China University of Technology, Guangzhou 510640, China

[c] Johan Gadolin Process Chemistry Centre, Laboratory of Natural Materials Technology, Åbo Akademi University, Turku FI-20500, Finland

Corresponding authors

* Tianjin Key Laboratory of Pulp and Paper, Tianjin University of Science & Technology, Tianjin 300457, China. Email: qingxihou@tust.edu.cn (Q. X. Hou); wei.liu2009@hotmail.com (W. Liu)

Abstract

The microfibrils of wood pulp fibers in plant cell wall with an intrinsically regular and interlaced arrangement offer a stable porous structure. They could also provide outstanding mechanical strength and promote conductivity for Si-based materials. Upon these benefits, a method using wood pulp fibers to fabricate SiO_2/C composite is proposed. In this work, the alkali pretreatment interfering hydrogen bonds in wood pulp fibers *in situ* results in an enlarged spatial distance among cellulose microfibrils, exposing more free-surface. This empowered homogenously inlaid SiO_2 distribution along the carbon skeleton in the subsequent carbonization process. A highly mesoporous and the tubular morphology was achieved in the fabricated SiO_2/C composite. Furthermore, a high initial coulombic efficiency of 84.9% and reversible specific capacity of 1130 mAh g^{-1} with a coulombic efficiency of 98.8% after 200 cycles at a current density of 0.1 A g^{-1} was obtained.

Keywords: Cellulose, Wood pulp fibers, SiO_2/C composite, Alkali pretreatment

1. Introduction

Lithium-ion batteries (LIBs) with characteristics of high energy density and environmental friendliness have attracted growing attention for electric energy storage in versatile fields such as mobile electronics and electric vehicles (Chen et al., 2017b; Shi et al., 2017; Tao et al., 2017). Abundant materials have been explored to replace graphite as the anode materials for LIBs to endow LIBs with a high specific capacity and cycle performance (Roy et al., 2016). Within the family of anode materials, Si-based materials, *i.e.*, SiO_x (x = 0, 1, 2), become a promising candidate mainly due to their high theoretical specific capacity. The coexistence of the irreversible and reversible lithiation mechanisms is well established in SiO_x-based anode (Equation 1a-c) (Favors et al., 2014). It allows a favorable achievement of a better cycling performance of the SiO_2-based anode than that of the pure Si-based anode due to the *in situ* formation of Li_4O_2 and Li_4SiO_4 serving as buffer media to suppress volume change (Chang et al., 2012; Zeng et al., 2018). Moreover, the inherent detriments of Si-based materials, such as poor electronic conductivity and low ion diffusivity, hamper the application of SiO_2-based anode (Xiao et al., 2019; Xu et al., 2018). SiO_2/C composites were designed to mitigate the abovementioned problems (Luo et al., 2015).

$$SiO_x + yLi^+ + ye^- \rightarrow Si + Li_yO_x \quad (1\text{-a})$$

$$yLi^+ + SiO_x \rightarrow Li_ySiO_x \quad (1\text{-b})$$

$$Li^+ + Si + xe^- \leftrightarrow Li_xSi \quad (1\text{-c})$$

Wood pulp fibers, one type of abundant and sustainable natural carbon-rich resources, supply a promising bio-template in the fabrication of energy storage composites (Tonoli et al., 2010). Gao's group (Yang et al., 2014) applied wood pulp fibers to assemble a novel MnO/C composite

possessing a high discharge capacity, stable cycle stability, and excellent rate performance. This is because the mesoporous structures of wood pulp fibers in plant cell wall was well preserved after carbonization (Luo et al., 2017). Additionally, it could be served as ion diffusion channels of the designate electrochemical energy storage materials during the charge and discharge processes. Similarly, Kim et al. proved (Kim et al., 2018b) that an improved electrochemical performance was achieved by utilizing naturally hierarchical mesoporous structure of wood pulp fibers functioning as electron paths. The macro- and micro-pores in carbon fibers originated from wood fibers had insufficient space for metal oxide to alleviate its volume expansion during lithiation and de-lithiation processes (Zhang et al., 2020). In addition, the unique micro-nano structure of porous carbon derived from wood pulp fibers could not only reduce the first irreversible capacity loss by limiting the contact between the electrode and electrolyte, but also enhance the specific capacity by accelerating the transfer of electrons and ions through nanopores (Zheng et al., 2016). Owing to the amorphous structure, large carbon interlayer, and fibrous morphology with hollow constructions, wood pulp fibers offered the carbon materials with remarkable electrochemical performance with favourable lithium/sodium ion storage and efficient transfer (Zhang et al., 2019). Based on the above, using wood pulp fibers to fabricate SiO_2/C composite is worth considering.

However, in order to facilitate storage and transportation, the wood pulp fibers have to be subjected to pressing and drying. This caused the deformation of the fibers, *i.e.*, pore collapse and lumen disappearance (Hribernik et al., 2016; Kimura et al., 2014). It further turns to insufficient space for ion transport as it will be used to fabricate SiO_2/C composite as the current state. In addition, the cell wall of wood pulp fibers is composed of a large number of cellulose molecular

chains which are arranged and aggregated sequentially. The aggregation of cellulose molecular chains results in two states: crystalline region and non-crystalline region (*i.e.* amorphous region). Particularly in the crystalline region, cellulose chains are tightly packed at the presence of inter-hydrogen bonds, causing low SiO_2 load from the low absorption rate of the precursor solution. An appropriate pretreatment is highly demanding to interfere the crystalline region and reopen the cell lumen in wood pulp fibers for fabricating SiO_2/C composites as high-performance anode material for LIBs.

Alkali treatment is well recognized in modifying the structure and properties of wood pulp fibers (Fink et al., 1999; Ishikura et al., 2010; Nakano, 2010; Zhang et al., 2005), because of its effects on the crystallinity and supermolecular structure of cellulose (Dinand et al., 2002; Eronen et al., 2009; Nie et al., 2018). It opens up a totally new avenue in the preparation of porous carbon scaffolds by offering the increased wrinkles and pores on the surface of the fibers. Moreover, the high SiO_2 load in the SiO_2/C composite can be obtained due to both the decrease in the total crystallinity (*i.e.*, the sum of the degrees of crystallinity for cellulose I and cellulose II) and the increased exposure of the accessible surface of wood pulp fibers after alkali treatment (Chen et al., 2017a; Halonen et al., 2013; Hribernik et al., 2016).

In the present work, a novel fabrication method of SiO_2/C composite by *in situ* synthesized method was established. The wood pulp fibers were pretreated with different concentration levels of alkali solution before immersing in the tetraethoxysilane (TEOS) ethanol solution. The exposure of more hydroxyl groups and the tubular morphology of wood pulp fibers can be achieved after alkali pretreatment. This endowed the homogeneous distribution of the silicon element on the

surface and inner wall of the tubular SiO_2/C composite after carbonization. Both inner and outer silica layers could participate in the lithiation reaction by using the composite as anode material for LIBs. The capacity of liquid retention for the pretreated pulp fibers and the changes in the crystallinity of cellulose were both investigated. Then the micro-morphology, crystal structure and porous properties of the SiO_2/C composites prepared with the pretreated pulp fibers as carbon skeleton were analyzed. At last, the electrochemical properties of the SiO_2/C composites were further characterized. The present work successfully demonstrated the feasibility of wood pulp fibers by *in situ* regulation using alkali solution as carbon skeleton to prepare the tubular SiO_2/C composites, offering one potential high-performance anode material for LIBs.

2. Experimental

2.1 Selection, dispersion, and alkali pretreatment of natural lignocellulosic fibers

The natural lignocellulosic fibers used in this work were from commercial bleached *Pinus radiata* kraft pulp made in Chile, of which the content of α-cellulose and ISO brightness were 89.42% and 85.98%, respectively, and the average fiber length and width were 2.32 mm and 33.1 μm, respectively.

The equivalent of 200 g oven-dry wood pulp fibers was taken and well dispersed in 20 L deionized (DI) water by using a Valley beater (No. 2505, KRK Co., Japan) at room temperature and atmosphere pressure for 30 min. It was further thickened using an 80-mesh polycotton bag until the dryness reached about 30%, and sealed in a plastic bag and stored at about 4 °C.

The wood pulp fibers were separately immersed in 0, 5, 10, 15, and 17.5 wt% NaOH solution

at a solid to liquid ratio of 1:100 (g/mL) at room temperature and a stirring speed of 600 rpm for 1 h. After the alkali pretreatment, the wood pulp fibers were rigorously washed with DI water until the pH of the filtrate was neutral. The pulp was then thickened once again to a dryness of about 30%. It was sealed in a plastic bag and stored at about 4 °C for later use.

2.2 Water retention value (WRV) of the wood pulp fibers

The WRV of the wood pulp fibers was principally measured according to the standard method of ISO 23714 (2014). The equivalent of about 300 mg oven-dry wood pulp fibers pretreated with NaOH solution was selected and immersed in 300 mL of DI water for 1h at room temperature, then centrifuged at (3000 ± 50) g for (1800 ± 30) s in a centrifuge (D-37520, SIGMA Laborzentifugen, German). After centrifugation, the WRV was calculated using the following equation (2):

$$WRV = m_2 / m_1 - 1 \quad (2)$$

where m_2 and m_1 are the weights of the wood pulp fibers before and after oven-drying in g, respectively.

2.3 Crystallinity index (CrI) of the wood pulp fibers

CrI is an index that can reflect the content of crystalline regions and accessibility of the wood pulp fibers. In the present work, an X-ray diffractometer (XRD-6100, Shimadzu Co., Japan) with a Cu target and a scan speed of 0.02 °/min was used to determine the total *CrI* of the wood pulp fibers, which was the sum of crystallinity for cellulose I and cellulose II. The *CrI* for cellulose I and cellulose II was separately estimated using the following equation (3) in the literature (Buschle-Diller and Zeronian, 1992):

$$CrI = (I_2 - I_1) / I_2 \quad (3)$$

where I_1 is the intensity at the minimum (between $2\theta = 18°$ and 19° for cellulose I and between $2\theta = 13°$ and 15° for cellulose II), and I_2 is the intensity of the crystalline peak at the maximum (between $2\theta = 22°$ and 23° for cellulose I and between $2\theta = 18°$ and 22° for cellulose II).

2.4 Preparation of SiO_2/C composites

The SiO_2/C composites derived from the wood pulp fibers were fabricated based on the combined sol-gel and heat treatment method (Dirican et al., 2015; Jia et al., 2017a; Jia et al., 2017b). The equivalent of 1.00 g oven-dry wood pulp fibers were first dispersed in 200 mL of the absolute ethanol at room temperature with a stirring speed of 800 rpm for 5 min. A fluffy and thin filter cake was made *via* suction filtration and solvent evaporation. The filter cake was further immersed into 40.0 mL of the silicon precursor solution (*i.e.*, 1.2 mol L^{-1} TEOS-ethanol solution) at room temperature and then taken out from the solution followed by drying in air. The silanol-cellulose composite cake was obtained by repeating the above immersing-drying process until the TEOS solution was fully consumed. The finally obtained silanol-cellulose composite cake was then aged in air at room temperature for 12 h to increase the degree of the silanol condensation. After the completion of the aging treatment, the silanol-cellulose composite cake was carbonized to yield the SiO_2/C composite in argon atmosphere at 600 °C and a heating rate 2 °C min^{-1} for 6 h. The resultant SiO_2/C composites were correspondingly denoted as 0, 5, 10, 15, and 17.5 wt%-SiO_2/C, respectively.

2.5 Characterization of the resultant SiO_2/C composites

The X-ray diffraction (XRD) patterns of the resultant SiO_2/C composites were recorded on an X-ray diffractometer (XRD-6100, Shimadzu Co., Japan). The Raman spectra of the SiO_2/C

155 composites were measured using a thermoelectrically cooled charge-coupled device (CCD)
156 detector (BTC 162E-532H, B&W TEK Optoelectronics Co., Shanghai, China) equipped with a 532
157 nm solid state laser (Power = 4 mW, Changchun New Industries Optoelectronics Technology Co.,
158 China). SEM images, elemental analysis and elemental mapping images were obtained using a
159 scanning electron microscope (JEOL JSM-IT300LV, Tokyo, Japan) equipped with an energy
160 dispersive X-ray spectrometer (EDX) (X-Max 20, Oxford, England). X-ray photoelectron
161 spectroscopy (XPS) (ESCALAB 250Xi, Thermo Scientific, USA) was carried out on 0, 15 and
162 17.5 wt%-SiO_2/C composites, respectively.

163 The surface features and pore structures of 0, 15 and 17.5 wt%-SiO_2/C composites, namely
164 the Brunauer-Emmett-Teller (BET) specific surface area (SSA), pore size distribution based on
165 density functional theory model, and micropore volume based on t-plot method, were all recorded
166 using a SSA and pore size analyzer (ASIQM0000000-6, Quantachrome Instruments, USA).

167 *2.6 Electrochemical measurements of the SiO_2/C composites*

168 To conduct the electrochemical measurement of the SiO_2/C composites, it is necessary to
169 fabricate the working electrodes. The as-prepared SiO_2/C composite was mixed together with both
170 acetylene black acting as a conductive agent and polyvinylidene fluoride (PVDF) serving as a
171 binder at a weight ratio of 70:20:10. The obtained uniform slurry was then coated onto pure copper
172 foils with a thickness of about 10 μm and dried in a vacuum oven at 120 °C for 24 h. The loading
173 mass of the active material, *i.e.*, the SiO_2/C composite, was about 1.9 mg cm^{-2}. The dried copper
174 foils with the active material coating were cut into small disks with a diameter of 16 mm. The
175 lithium metal disks with the same diameter were used as both the counter and reference electrodes.

The electrolyte was made by dissolving 1.0 mol L^{-1} lithium hexafluorophosphate ($LiPF_6$) in the mixture of ethylene carbonate (EC), dimethyl carbonate (DMC) and ethyl methyl carbonate (EMC) at a volume ratio of 1:1:1. A Celgard 2400 porous membrane was used as the separator. At last, CR2032 coin-type cells were assembled in a gloves box (Lab2000, Etelux Co., China) filled with high-purity Argon (H_2O < 0.01 ppm, O_2 < 0.01 ppm).

Cyclic voltammogram (CV) measurements were carried out using a CHI660D electrochemical workstation (CH instruments Co., China) in a voltage range of 0.01–3.0 V at a scanning rate of 1 mV s^{-1}. Electrochemical impedance spectroscopy (EIS) in a frequency range from 0.1 MHz to 0.01 Hz at an amplitude ratio of 5 mV was also performed using the same CHI660D electrochemical workstation. Galvanostatic charge and discharge measurements were conducted by using a LANHE CT2001A electrochemical workstation (Wuhan Land Co., China) in the voltage range of 0.01–3.0 V at a current density of 0.1 A g^{-1}.

3. Results and discussion

3.1. Morphologies and accessibility of the alkali-swollen wood pulp fibers

The changes in the cellulosic crystalline structure of the wood pulp fibers after alkaline swelling at different levels of alkali concentration were recorded by XRD patterns, as shown in Fig. 1a. It can be found that the pattern of the control wood pulp fibers exhibited a sharp high peak at 2θ = 22.7° and two overlapped weaker diffraction peaks at 2θ = 15.0° and 16.3°, respectively, which are assigned to cellulose I (Liu and Hu, 2008). For the sample treated with 10 wt% NaOH solution, however, two additional distinctive diffraction peaks appeared at the position of 2θ = 12.0°

and $2\theta = 20.0°$, which are assigned to cellulose II, one kind of allomorph of cellulose I. Cellulose I gradually transformed into cellulose II in the application of alkali treatment. As is known, cellulose II has large accessible crystal surface as compared to cellulose I. Therefore, alkali pretreatment could enhance the accessibility and reactivity of the wood pulp fibers through changing the crystal structure of the cellulose (Ciolacu et al., 2012). Meanwhile, the total crystallinity of the cellulose distinctly decreased with raising the concentration of the NaOH solution used in the alkali pretreatment, as shown in Fig. 1b. The changes in the surface morphology of the wood pulp fibers were captured by using SEM and depicted in Fig. S1. The alkaline swelling rendered the morphological changes of the wood pulp fibers from ribbon-like configuration to rod-like one with coarse surface at the presence of wrinkles and granulations. The resultant increase in the superficial area accordingly enhanced the accessibility and reactivity of the wood pulp fibers.

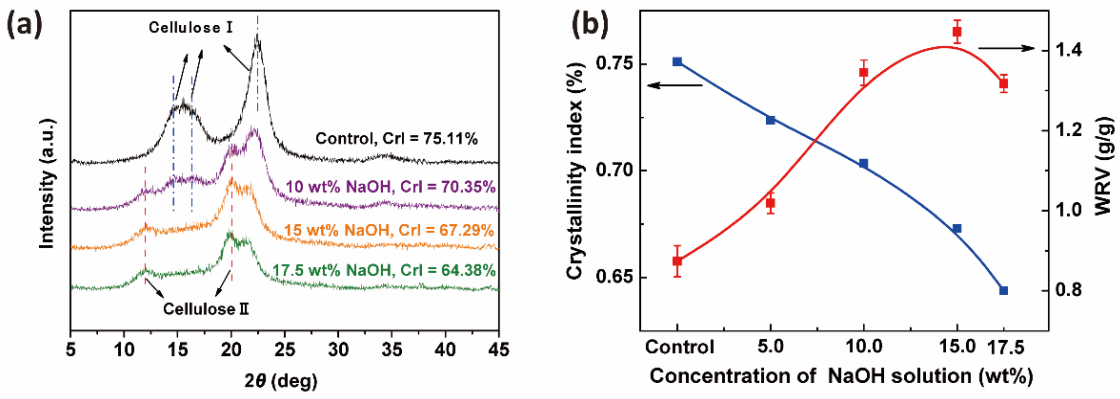

Fig. 1. (a) XRD patterns of wood pulp fibers pretreated with NaOH solution at different levels of concentration, (b) Effects of alkali pretreatment on the total crystallinity and WRV of wood pulp fibers.

Fig. 1b also shows that the higher the concentration of alkali solution, the higher the WRV of wood pulp fibers, except for the sample pretreated with 17.5 wt% NaOH solution. The alkaline

swelling on the wood pulp fibers brought higher cellulose accessibility both in amorphous and crystalline regions than water swelling, which was manifested by the improvement in the WRV of wood pulp fibers. However, an excessively high concentration of NaOH solution can cause a decrease in the number of water molecules introduced into cellulose by hydrated alkali ions or hydrated dipole ions, resulting in the weakening of the swelling effect of alkali solution on cellulose. It is apparent from the above that the concentration of alkali solution played a prominent role in the alkaline swelling of wood pulp fibers. It is of vital importance for wood pulp fibers to have a higher WRV in the process of preparing SiO_2/C composites by using the method of combining sol-gel and heating. This is because there would be more free hydroxyl groups are exposed in the swollen cellulose chains, which is very much beneficial to the retention and uniform distribution of SiO_2 in the target SiO_2/C composite.

3.2. Morphologies and structures of the SiO_2/C composites

The 15 wt%-SiO_2/C composite prepared from the NaOH-swollen wood pulp fibers still maintained the same rod-like structure as that before carbonization (Fig. 2a), and the 0 wt%-SiO_2/C composite derived from untreated wood pulp fibers showed as ribbon-like (Fig. 2c). It means all SiO_2/C composites would conserve their original morphology after carbonization. It can be concluded that alkali treatment is effective to regulate the morphology of SiO_2/C composites. The cross-sectional images of the corresponding SiO_2/C composites are shown in Fig. 2b and d, respectively, indicating that the larger lumen was only found in 15 wt%-SiO_2/C composite. Overall, 15 wt%-SiO_2/C composite possessed tubular morphology, which is preferred to make lithium diffusion distance shorter and to have enough space to prevent the pulverization of silicon (Su et

al., 2014; Yoo et al., 2012). The N_2 absorption-desorption isotherm and pore size distribution curves of these two kinds of SiO_2/C composites, *i.e.*, 0 and 15 wt%-SiO_2/C composite, are presented in Fig. 2e and f, and the porous properties of these SiO_2/C composites are summarized in Table S1. 15 wt%-SiO_2/C composite presented a relatively higher SSA and a total pore volume than those of 0 wt%-SiO_2/C composite. This could be attributed to the fact that the surface of 15 wt%-SiO_2/C was rougher than that of 0 wt%-SiO_2/C (insets in Fig. 2a and c). In addition, although Table S1 and the insets in Fig. 2e and f reveal that these two kinds of the composite contained micro- (< 2 nm) and meso-pores (2–50 nm), and the 15 wt%-SiO_2/C composite exhibited a higher V_{meso}/V_{total} ratio (92.81%). The high SSA for 15 wt%-SiO_2/C composite could facilitate the infiltration of liquid electrolyte into the composite electrode and thus promoted the charge transfer process (Hou et al., 2016; Shen et al., 2018), and sufficient pore volume is beneficial to accommodate the volumetric expansion of silica (Kim et al., 2018a). The thin and porous cell wall and large lumen of 15 wt%-SiO_2/C composite might improve the electrochemical energy storage (Li et al., 2013; Mhamane et al., 2018; Yun et al., 2015), and accelerated the liquid-electrolyte penetration, ion diffusion and transfer (Mhamane et al., 2018). The stable tubular structure could be beneficial to forming a stable solid-electrolyte-interphase (SEI) film, preventing irreversible insertion reaction of lithium-ion into the carbon structure (Cao et al., 2012; Tao et al., 2017; Yao et al., 2003).

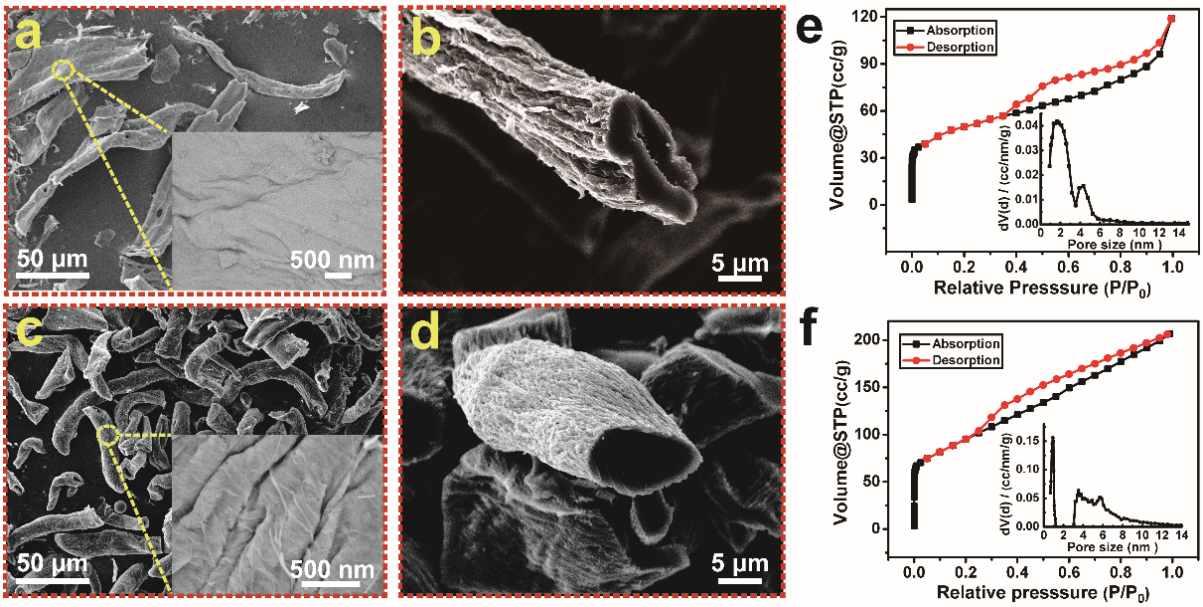

Fig. 2. SEM images of the resultant SiO_2/C composites for (a) 0 wt%-SiO_2/C and (c) 15 wt%-SiO_2/C with different magnification, and the cross section of (b) 0 wt%-SiO_2/C and (d) 15 wt%-SiO_2/C; N_2 absorption-desorption isotherm and pore size distribution curves (inner plot) for (e) 0 wt%-SiO_2/C composite and (f) 15 wt%-SiO_2/C composite.

The hypothesis, *i.e.*, high WRV of wood pulp fibers enhancing the retention and uniform distribution of SiO_2 in the target SiO_2/C composite, was also confirmed by the EDX peaks of C, O, and Si element in the SiO_2/C composites, as shown in Fig. 3. The surface of 15 wt%-SiO_2/C composite presented more Si element (12.39%) than that of the control sample (4.92%), as shown in Fig. 3a-b. This demonstrates the fact that the SiO_2 load in SiO_2/C composites was correlated with the cellulose accessibility of wood pulp fibers. The higher the cellulose accessibility, the greater the SiO_2 load. Moreover, both the axial and cross-sectional surfaces of 15 wt%-SiO_2/C composite presented almost the same Si element distribution (Fig. 3b-c), indicating almost the same

silicon accessibility to the axial and cross-section surfaces of the cell wall for NaOH-swollen wood pulp fibers. It is indicated that alkali pretreatment would promote the homogeneous distribution of the silicon element on the surface and inner wall of the tubular SiO_2/C composite after carbonization. When the composite is used as the anode material for LIBs, both inner and outer silica layers could participate in the lithiation reaction to accelerate liquid-electrolyte penetration and Li-ion charge/discharge. The elemental mappings (Fig. 3d-e) indicate that C, O and Si elements were all distributed uniformly throughout the SiO_2/C composite. It can be summarized that it is feasible to increase the silica content and make it uniformly distributed throughout the SiO_2/C composite prepared from NaOH-swollen wood pulp fibers by means of alkali pretreatment.

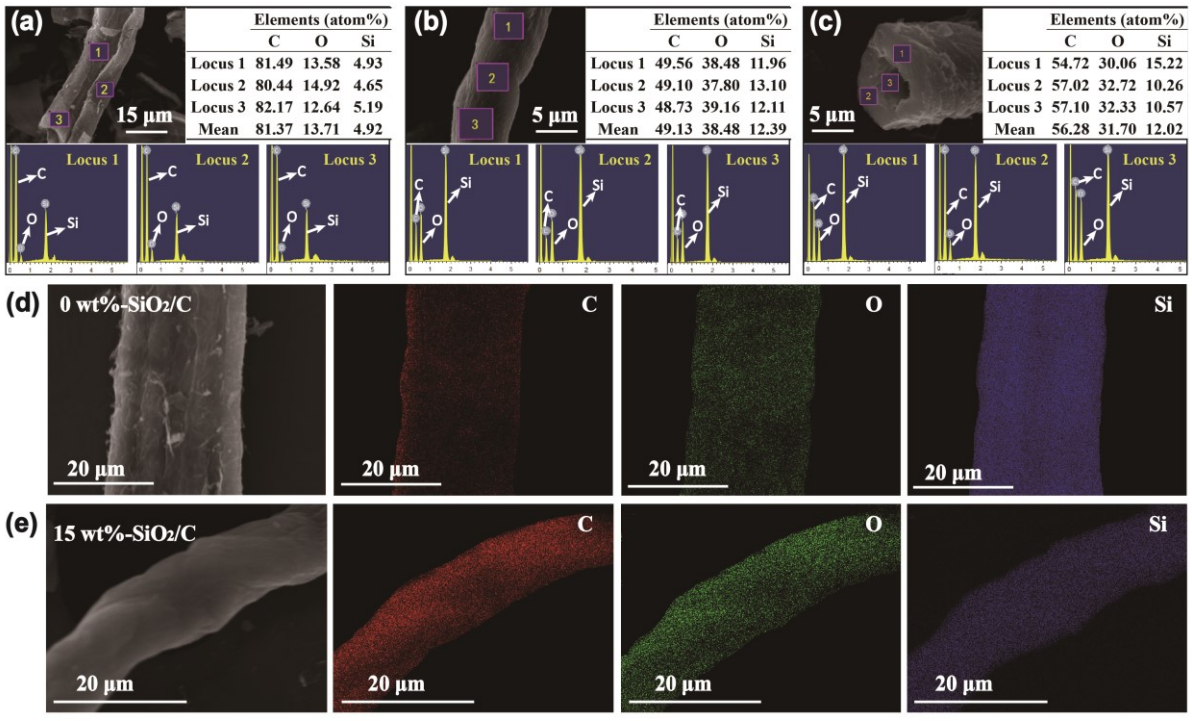

Fig. 3. Axial EDX patterns for the composites of (a) 0 wt%-SiO_2/C and (b) 15 wt%-SiO_2/C; the cross-sectional EDX patterns for (c) 15 wt%-SiO_2/C composite; EDX elemental mappings of C, O, and Si in (d) 0 wt%-SiO_2/C composite and (e) 15 wt%-SiO_2/C composite.

Fig. 4a presents the XRD patterns of as-prepared 0, 15 and 17.5 wt%-SiO_2/C composites. All the composites possessed amorphous or low crystallinity features due to no sharp diffraction peaks in the XRD patterns. A broad peak located in 2θ range of 16–30° was associated with amorphous SiO_2, and the weak diffraction peak around 43° was ascribed to disordered carbon (Kim et al., 2018b; Li and Zhou, 2012). There was no obvious difference in the XRD pattern between 0 and 17.5 wt%-SiO_2/C composites except for the fact that 15 wt%-SiO_2/C composite exhibited a strong diffraction peak arising from amorphous SiO_2 (Fig. 4a). In addition, there was no distinguishable diffraction peak in the XRD patterns attributing to the Si, indicating that the SiO_2 wouldn't be reduced to Si during the process of preparing SiO_2/C composite. It has been proved that amorphous SiO_2 has higher electrochemical activity than SiO_2 with crystalline cluster (Lv et al., 2013). The Raman spectra of three kinds of SiO_2/C composites (Fig. 4b) clearly show the D-band around 1360 cm^{-1} and the G-band around 1590 cm^{-1}, demonstrating the existence of disordered carbon and sp^2 graphitic carbon in the SiO_2/C composites, respectively (Mhamane et al., 2018; Zhu et al., 2017). The intensity ratios of D-band to G-band (I_D/I_G) for the selected three kinds of SiO_2/C composites were 0.72, 0.74 and 0.67, respectively, suggesting that the carbon in the SiO_2/C composites was endowed with a relatively high degree of graphitization due to the presence of SiO_2 in the composites, which could promote the growth of carbon upon heating (Agyeman et al., 2016; Shen et al., 2018). By far a carbon scaffold for improving the electrical conductivity of the prepared SiO_2/C composite is fabricated by using wood pulp fibers, regardless of whether wood pulp fibers were pretreated with or without NaOH solution. XPS was selected to further detect the surface chemical composition and chemical states of the prepared SiO_2/C composites, as shown in Fig. 4c-

f. The survey spectra (Fig. 4c) of each tested SiO_2/C composite contained four distinct bands at 103, 153, 284, and 532 eV, corresponding to Si 2p, Si 2s, C 1s, and O 1s, respectively, which indicates that silicon, carbon and oxygen were three dominant elements in the prepared SiO_2/C composites. The high-resolution C 1s spectrum of each SiO_2/C composite could be fitted to three bands by applying the curve-fitting procedure, as shown in Fig. 4d. The C1s peaks located at 284.8, 286.2 and 288.8 eV were attributed to the free carbon, C-O and C=O bonds in the SiO_2/C composites, respectively. Almost disappeared bands attributed to C-O and C=O bonds in the 17.5 wt%-SiO_2/C composite indicated that alkali pretreatment of the wood pulp fibers had a great influence on the formation of oxygen functional groups in the carbonization process. Typical high-resolution Si 2p and O 1s spectra of the selected three kinds of the composites are depicted in Fig. 4e and f. The bands at 103.51 eV for Si 2p and 532.5 eV for O 1s mean the silicon element in the form of silicon dioxide existed in the prepared SiO_2/C composites (Chou et al., 2018; Xiao et al., 2019). It is again confirmed that SiO_2 could not be reduced to Si in the preparation of the SiO_2/C composite.

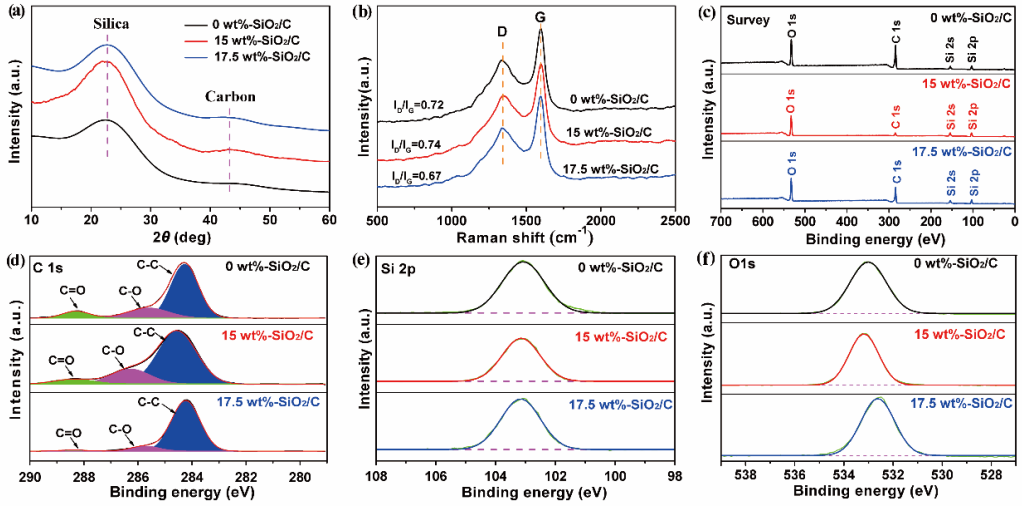

Fig. 4. (a) XRD patterns, (b) Raman spectra, (c) XPS survey spectra, (d) high-resolution C 1s XPS spectra, (e) high-resolution Si 2p XPS spectra, and (f) high-resolution O 1s XPS spectra of the resultant SiO_2/C composites.

3.3. Electrochemical properties of the SiO_2/C composites

The cycling stability for 0 and 15 wt%-SiO_2/C composites was evaluated *via* galvanostatic charging/discharging in the potential range of 0.01−3.0 V at a constant current density of 100 mA g^{-1}. As shown in Fig. 5a and b, 0 and 15 wt%-SiO_2/C composites exhibited charge/discharge capacity of 400/1060 and 1275/1502 mAh g^{-1}, respectively in the first cycle. The capacity loss in the initial cycle can be attributed to the irreversible consumption of electrolyte, including the formation of the SEI film on the surface of electrode, the reduction of SiO_2 and the formation of elemental silicon and a series of silicates (Shen et al., 2018; Yang et al., 2017). The initial coulombic efficiency (CE) of 15 wt%-SiO_2/C composite was 84.9% at 100 mA g^{-1}, much higher than that of 0 wt%-SiO_2/C composite (37.7%), as well as other Si/C composites displayed in Table 1. This is attributed to the short lithium diffusion distance and a high mesoporous proportion for the tubular structure of porous carbon derived from the NaOH-swollen wood pulp fibers, thus reducing the consumption of lithium ions to form the SEI film and the insertion of irreversible lithium into SiO_2/C composite (Kim et al., 2018b; Li and Zhou, 2012). Moreover, the charge/discharge curves for 0 wt%-SiO_2/C composite remained similar in shape with a small decrease in the capacity from the 5^{th} to the 200^{th} cycle (Fig. 5a), being similar to those for 15 wt%-SiO_2/C composite (Fig. 5b). The average CE from the 5^{th} to the 200^{th} cycle for both 0 and 15 wt%-SiO_2/C composites reached 98.8%, indicating that these two kinds of SiO_2/C composites presented

an excellent cycling stability (Fig. 5c). This is ascribed to the carbon derived from the wood pulp fibers that could provide a reliable buffer layer and good mechanical support to the SiO_2 layer (Shen et al., 2018) whether or not the wood pulp fibers were pretreated with NaOH solution. The reversible specific capacity of 15 wt%-SiO_2/C composite (1130 mAh g^{-1}) was much higher than that of 0 wt%-SiO_2/C composite (307 mAh g^{-1}) after 200 cycles due to a higher SiO_2 content of the former. Moreover, the electrochemical performance of 15 wt%-SiO_2/C composite was also comparable to those of recently reported SiO_x/C ($0 \leq x \leq 2$) anode materials with cellulose as carbon resource (Table 1). The galvanostatic charge/discharge voltage profiles of 15 wt%-SiO_2/C composite at 400 mA g^{-1} is shown in Fig. S2.

Fig S3 and Fig. 5d show the CV curves of the first three cycles for 0 and 15 wt%-SiO_2/C composites, respectively in the potential range of 0.0−3.0 V *vs.* Li/Li^+ at a scanning rate of 1.0 mV s^{-1}. According to previous studies (Favors et al., 2014; Jiang et al., 2013; Li et al., 2015; Schroder et al., 2012), the reduction peaks at about 1.25 and 0.43 V in the first cathodic sweep can be all ascribed to the decomposition of electrolyte on the composite surface, the irreversible formation of the SEI film, the reduction of SiO_2, and the formation of elemental silicon and a series of silicates. There is more conspicuous peak at about 0.43 V in the 0 wt%-SiO_2/C composite than that in the 15 wt%-SiO_2/C composite. It means that more irreversible loss of capacity during the first cycle happened in the 0 wt%-SiO_2/C composite, which could be also concluded by the galvanostatic charging/discharging curves (Fig. 5a and b). Notably, the reduction peak around 1.25 and 0.43 V in the CV curves of all SiO_2/C composites disappeared in the subsequent curves (Fig S3 and Fig. 5d), suggesting that stable SEI film was formed for these two kinds of SiO_2/C composites after the

first cycle. When the potential got lower to 0.1 V in the cathodic scan, a sharp reduction peak could be observed, which is attributed to the lithiation of silicon to form a Li_xSi alloy (Dirican et al., 2015; Kim et al., 2015). The charging branch showed a broad oxidation peak around 0.5 V due to the extraction of ions from Li_xSi. Obviously, the oxidation peak exhibited an enhanced intensity during the anodic sweep, which can be mainly attributed to the gradual activation process of anode.

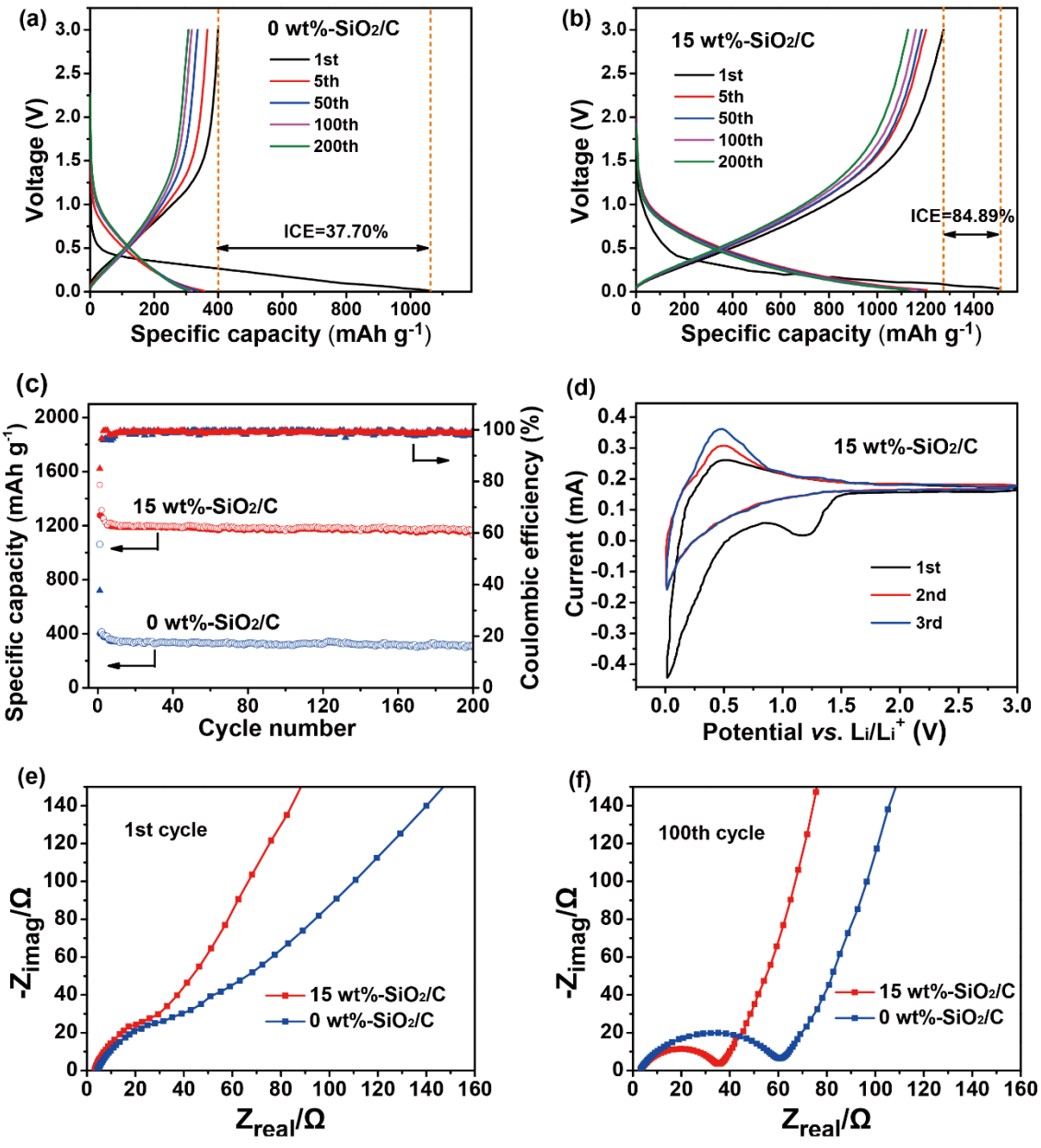

Fig. 5. Galvanostatic charge/discharge voltage profiles of (a) 0 wt%-SiO_2/C composite and (b) 15 wt%-SiO_2/C composite; (c) cycling performance of 0 wt%-SiO_2/C and 15 wt%-SiO_2/C composites at 100 mA g^{-1}; (d) CV curves of 15 wt%-SiO_2/C composite; and Nyquist plots for 0 and 15 wt%-SiO_2/C composites after (e) the 1st and (f) the 100th charge/discharge cycles.

Table 1 Comparison of electrochemical performance for various SiO_x/C anode materials.

Cellulose form	Materials	Electrochemical performance			References
		Current density	Reversible specific capacity	Initial CE	
Cellulose solution	Core-shell structured Si@SiO_2/C composite	420 mA g^{-1}	1071 mA h g^{-1} after 200 cycles	61.0% at 100 mA g^{-1}	(Shen et al., 2018)
Cellulose nanofibers	Si/C composite with network structure	400 mA g^{-1}	1594 mA h g^{-1} after 200 cycles	78.8% at 100 mA g^{-1}	(Kim et al., 2017)
Cellulose nanofibers	textile-like carbon wrapped Si/C composite	2 A g^{-1}	1097 mA h g^{-1} after 200 cycles	73.8% at 100 mA g^{-1}	(Kim et al., 2018b)
Filter paper	Nanofibrous SiO_2/C composite	100 mA g^{-1}	400.4 mA h g^{-1} after 200 cycles	45.9% at 100 mA g^{-1}	(Jia et al., 2017b)
NaOH-swollen wood pulp fiber	Tubular SiO_2/C composite	100 mA g^{-1}	1130 mA h g^{-1} after 200 cycles	84.9% at 100 mA g^{-1}	This work
		400 mA g^{-1}	1056.4 mA h g^{-1} after 200 cycles	76.02% at 400 mA g^{-1}	

Electrochemical impedance spectroscopy (EIS) tests were employed to explore the impedance of 0 and 15 wt%-SiO_2/C composites at a frequency range from 0.1 MHz to 0.01 Hz at an amplitude ratio of 5 mV. Nyquist plots at the fresh status and the 100^{th} cycle for 0 and 15 wt%-SiO_2/C composites were respectively obtained. As shown in Fig. 5e, the depressed semicircle could not be observed from the curves of 0 and 15 wt%-SiO_2/C composites at fresh status, which resulted from the inexistence of the SEI film in fresh cells. After 100 cycles (Fig. 5f), however, 15 wt%-SiO_2/C

composite exhibited a smaller semicircle at the medium-frequency zone, suggesting a smaller charge transfer resistance on the electrode/electrolyte as compared to that of 0 wt%-SiO_2/C composite (Kim et al., 2015). Overall, the alkaline swelling of wood pup fibers would endow the resultant SiO_2/C composites with an excellent electrochemical performance.

4. Conclusions

The carbon skeleton of the SiO_2/C composite derived from wood pulp fibers could provide a reliable buffer layer and good mechanical support to the SiO_2 layer whether or not wood pulp fibers were pretreated with NaOH solution, which could endow the SiO_2/C composite used as the anode material for LIBs with excellent cycling stability. The resultant SiO_2/C composite remained the morphology of wood pulp fibers, and the tubular SiO_2/C composite derived from NaOH-swollen wood pulp fibers, *e.g.*, 15 wt%-SiO_2/C composite, had a silica load of 12.39% and a reversible specific capacity of 1130 mAh g^{-1} at 100 mA g^{-1} after 200 cycles, behaving better performance than the reference, *i.e.*, 0 wt%-SiO_2/C composite (307 mAh g^{-1}). The improvement is proposed with the association of the improved accessibility of wood pulp fibers to the liquid silica precursor in the process of alkaline swelling. High mesoporous proportion and the tubular morphology of prepared 15 wt%-SiO_2/C composite could shorten the lithium diffusion distance and reduce the consumption of lithium ions to form the SEI film obtaining a high initial coulombic efficiency. This work demonstrated the feasibility of regulating the morphology of wood pulp fibers by pretreatment, *e.g.*, alkali pretreatment, in order to obtain SiO_2/C composites with ideal morphology and excellent electrochemical performance.

Acknowledgements

This work was financially supported by State Key Laboratory of Pulp and Paper Engineering (201823).

Appendix A. Supplementary data

Supplementary data associated with this article can be found, in the online version.

References

Agyeman, D.A., Song, K., Lee, G.H., Park, M., Kang, Y.M., 2016. Carbon-coated Si nanoparticles anchored between reduced graphene oxides as an extremely reversible anode material for high energy-density Li-ion battery. Adv. Energy Mater. 6, 1600904.

Buschle-Diller, G., Zeronian, S.H., 1992. Enhancing the reactivity and strength of cotton fibers. J. Appl. Polym. Sci. 45, 967–979.

Cao, Y.L., Xiao, L.F., Sushko, M.L., Wang, W., Schwenzer, B., Xiao, J., Nie, Z.M., Saraf, L.V., Yang, Z.G., Liu, J., 2012. Sodium ion insertion in hollow carbon nanowires for battery applications. Nano Lett. 12, 3783–3787.

Chang, W.S., Park, C.M., Kim, J.H., Kim, Y.U., Jeong, G., Sohn, H.J., 2012. Quartz (SiO_2): a new energy storage anode material for Li-ion batteries. Energ. Environ. Sci. 5, 6895–6899.

Chen, H., Yu, Y., Zhong, T.H., Wu, Y., Li, Y.J., Wu, Z.H., Fei, B.H., 2017a. Effect of alkali treatment on microstructure and mechanical properties of individual bamboo fibers. Cellulose 24, 333–347.

Chen, T., Hu, J.Z., Zhang, L., Pan, J., Liu, Y.Y., Cheng, Y.T., 2017b. High performance binder-free SiOx/C composite LIB electrode made of SiOx and lignin. J. Power Sources 362, 236–242.

Chou, C.Y., Kuo, J.R., Yen, S.C., 2018. Silicon-based composite negative electrode prepared from recycled silicon-slicing slurries and lignin/lignocellulose for Li-ion cells. ACS Sustain. Chem. Eng. 6, 4759–4766.

Ciolacu, D., Pitol, L., Ciolacu, F., 2012. Studies concerning the accessibility of different allomorphic forms of cellulose. Cellulose 19, 55–68.

Dinand, E., Vignon, M., Chanzy, H., Heux, L., 2002. Mercerization of primary wall cellulose and its implication for the conversion of cellulose I → cellulose II. Cellulose 9, 7–18.

Dirican, M., Yildiz, O., Lu, Y., Fang, X.M., Jiang, H., Kizil, H., Zhang, X.W., 2015. Flexible binder-free silicon/silica/carbon nanofiber composites as anode for lithium-ion batteries. Electrochim. Acta 169, 52–60.

Eronen, P., Osterberg, M., Jaaskelainen, A.S., 2009. Effect of alkaline treatment on cellulose supramolecular structure studied with combined confocal Raman spectroscopy and atomic force microscopy. Cellulose 16, 167–178.

Favors, Z., Wang, W., Bay, H.H., George, A., Ozkan, M., Ozkan, C.S., 2014. Stable cycling of SiO_2 nanotubes as high-performance anodes for lithium-ion batteries. Sci. Rep. 4, 4605.

Fink, H.P., Walenta, E., Kunze, J., 1999. The structure of natural cellulosic fibres-Part 2. The supermolecular structure of bast fibres and their changes by mercerization as revealed by X-ray diffraction and C-13-NMR-spectroscopy. Papier 53, 534–542.

Halonen, H., Larsson, P.T., Iversen, T., 2013. Mercerized cellulose biocomposites: a study of influence of mercerization on cellulose supramolecular structure, water retention value and tensile properties. Cellulose 20, 57–65.

Hou, G.L., Cheng, B.L., Cao, Y.B., Yao, M.S., Li, B.Q., Zhang, C., Weng, Q.H., Wang, X., Bando, Y., Golberg, D., Yuan, F.L., 2016. Scalable production of 3D plum-pudding-like Si/C spheres: towards practical application in Li-ion batteries. Nano Energy 24, 111–120.

Hribernik, S., Kleinschek, K.S., Rihm, R., Ganster, J., Fink, H.P., Smole, M.S., 2016. Tuning of cellulose fibres' structure and surface topography: Influence of swelling and various drying procedures. Carbohyd. Polym. 148, 227–235.

Ishikura, Y., Abe, K., Yano, H., 2010. Bending properties and cell wall structure of alkali-treated wood. Cellulose 17, 47–55.

Jia, D.L., Li, X., Huang, J.G., 2017a. Bio-inspired sandwich-structured carbon/silicon/titanium-oxide nanofibers composite as an anode material for lithium-ion batteries. Compos. Part A-Appl. S. 101, 273–282.

Jia, D.L., Wang, K., Huang, J.G., 2017b. Filter paper derived nanofibrous silica-carbon composite as anodic material with enhanced lithium storage performance. Chem. Eng. J. 317, 673–686.

Jiang, T., Zhang, S.C., Lin, R.X., Liu, G.R., Liu, W.B., 2013. Electrochemical characterization of cellular Si and Si/C anodes for lithium ion battery. International Int. J. Electrochem. Sci. 8, 9644–9651.

Kim, B., Ahn, J., Oh, Y., Tan, J., Lee, D., Lee, J.K., Moon, J., 2018a. Highly porous carbon-coated silicon nanoparticles with canyon-like surfaces as a high-performance anode material for Li-ion batteries. J. Mater. Chem. A 6, 3028–3037.

Kim, H., Huang, X., Wen, Z., Cui, S., Guo, X., Chen, J., 2015. Novel hybrid Si film/carbon nanofibers as anode materials in lithium-ion batteries. J. Mater. Chem. A 3, 1947-1952.

Kim, J.M., Guccini, V., Kim, D., Oh, J., Park, S., Jeon, Y., Hwang, T., Salazar-Alvarez, G., Piao, Y.Z., 2018b. A novel textile-like carbon wrapping for highperformance silicon anodes in lithium-ion batteries. J. Mater. Chem. A 6, 12475–12483.

Kim, J.M., Guccini, V., Seong, K.-d., Oh, J., Salazar-Alvarez, G., Piao, Y., 2017. Extensively interconnected silicon nanoparticles via carbon network derived from ultrathin cellulose nanofibers as high performance lithium ion battery anodes. Carbon 118, 8–17.

Kimura, M., Qi, Z.D., Fukuzumi, H., Kuga, S., Isogai, A., 2014. Mesoporous structures in never-dried softwood cellulose fibers investigated by nitrogen adsorption. Cellulose 21, 3193–3201.

Li, H., Zhou, H., 2012. Enhancing the performances of Li-ion batteries by carbon-coating: present and future. Chem. Commun. 43, 1201–1217.

Li, M.Q., Gu, J.W., Feng, X.F., He, H.Y., Zeng, C.M., 2015. Amorphous-silicon@silicon oxide/chromium/carbon as an anode for lithium-ion batteries with excellent cyclic stability. Electrochim. Acta 164, 163–170.

Li, Z., Xu, Z.W., Tan, X.H., Wang, H.L., Holt, C.M.B., Stephenson, T., Olsen, B.C., Mitlin, D., 2013. Mesoporous nitrogen-rich carbons derived from protein for ultra-high capacity battery anodes and supercapacitors. Energ. Environ. Sci. 6, 871–878.

Liu, Y.P., Hu, H., 2008. X-ray diffraction study of bamboo fibers treated with NaOH. Fiber. Polym. 9, 735–739.

Luo, C., Zhu, H.L., Luo, W., Shen, F., Fan, X.L., Dai, J.Q., Liang, Y.J., Wang, C.S., Hu, L.B., 2017. Atomic-layer-deposition functionalized carbonized mesoporous wood fiber for high sulfur loading lithium sulfur batteries. ACS Appl. Mater. Inter. 9, 14801–14807.

Luo, F., Liu, B.N., Zheng, J.Y., Chu, G., Zhong, K.F., Li, H., Huang, X.J., Chen, L.Q., 2015. Review-nano-silicon/carbon composite anode materials towards practical application for next generation Li-ion batteries. J. Electrochem. Soc. 162, A2509–A2528.

Lv, P.P., Zhao, H.L., Wang, J., Liu, X., Zhang, T.H., Xia, Q., 2013. Facile preparation and electrochemical properties of amorphous SiO_2/C composite as anode material for lithium ion batteries. J. Power Sources 237, 291–294.

Mhamane, D., Kim, M.S., Park, B.H., Choi, H.S., Kim, Y.H., Aravindan, V., Phadkule, A., Kim, K.B., 2018. Orderly meso-perforated spherical and apple-shaped 3D carbon microstructures for high-energy supercapacitors and high-capacity Li-ion battery anodes. J. Mater. Chem. A 6, 6422–6434.

Nakano, T., 2010. Mechanism of microfibril contraction and anisotropic dimensional changes for cells in wood treated with aqueous NaOH solution. Cellulose 17, 711–719.

Nie, S.X., Zhang, C.Y., Zhang, Q., Zhang, K., Zhang, Y.H., Tao, P., Wang, S.F., 2018. Enzymatic and cold alkaline pretreatments of sugarcane bagasse pulp to produce cellulose nanofibrils using a mechanical method. Ind. Crop. Prod. 124, 435–441.

Roy, A.K., Zhong, M., Schwab, M.G., Binder, A., Venkataraman, S.S., Tomović, Ž., 2016. Preparation of a binder-free three-cimensional carbon foam/slicon composite as potential material for lithium ion battery anodes. ACS Appl. Mater. Inter. 8, 7343–7348.

Schroder, K.W., Celio, H., Webb, L.J., Stevenson, K.J., 2012. Examining solid electrolyte interphase formation on crystalline silicon electrodes: influence of electrochemical preparation and ambient exposure conditions. J. Phys. Chem. 116, 19737–19747.

Shen, D.Z., Huang, C.F., Gan, L.H., Liu, J., Gong, Z.L., Long, M.N., 2018. Rational design of Si@SiO_2/C composites using sustainable cellulose as a carbon resource for anodes in lithium-ion batteries. ACS Appl. Mater. Inter. 10, 7946–7954.

Shi, Z.Q., Jin, G.Q., Wang, J., Zhang, J., 2017. Free-standing, welded mesoporous carbon nanofibers as anode for high-rate performance Li-ion batteries. J. Electroanal. Chem. 795, 26–31.

Su, X., Wu, Q., Li, J., Xiao, X., Lott, A., Lu, W., Sheldon, B.W., Wu, J., 2014. Silicon-based nanomaterials for lithium-ion batteries: A Review. Adv. Energy Mater. 4, 375–379.

Tao, L., Zheng, Y.W., Zhang, Y.H., Ma, H., Di, M.W., Zheng, Z.F., 2017. Liquefied walnut shell-derived carbon nanofibrous mats as highly efficient anode materials for lithium ion batteries. RSC Adv. 7, 27113–27120.

Tonoli, G.H.D., Savastano, H., Fuente, E., Negro, C., Blanco, A., Lahr, F.A.R., 2010. Eucalyptus pulp fibres as alternative reinforcement to engineered cement-based composites. Ind. Crop. Prod. 31, 225–232.

Xiao, T.T., Zhang, W.F., Xu, T., Wu, J.X., Wei, M.D., 2019. Hollow SiO_2 microspheres coated with nitrogen doped carbon layer as an anode for high performance lithium-ion batteries. Electrochim. Acta 306, 106–112.

Xu, Q., Sun, J.K., Yin, Y.X., Guo, Y.G., 2018. Facile synthesis of blocky SiOx/C with graphite-like structure for high-performance lithium-ion battery anodes. Adv. Funct. Mater. 28, 1705235.

Yang, C.X., Gao, Q.M., Tian, W.Q., Tan, Y.L., Zhang, T., Yang, K., Zhu, L.H., 2014. Superlow load of nanosized MnO on a porous carbon matrix from wood fibre with superior lithium ion storage performance. J. Mater. Chem. A 2, 19975–19982.

Yang, T., Tian, X.D., Li, X., Wang, K., Liu, Z.J., Guo, Q.G., Song, Y., 2017. Double core-shell Si@C@SiO_2 for anode material of lithium-ion batteries with excellent cycling stability. Chem-Eur. J. 23, 2165–2170.

Yao, J., Wang, G.X., Ahn, J.H., Liu, H.K., Dou, S.X., 2003. Electrochemical studies of graphitized mesocarbon microbeads as an anode in lithium-ion cells. J. Power Sources 114, 292–297.

Yoo, J.K., Kim, J., Jung, Y.S., Kang, K., 2012. Scalable fabrication of silicon nanotubes and their application to energy storage. Adv. Mater. 24, 5452–5456.

Yun, Q.B., Qin, X.Y., Lv, W., He, Y.B., Li, B.H., Kang, F.Y., Yang, Q.H., 2015. "Concrete" inspired construction of a silicon/carbon hybrid electrode for high performance lithium ion battery. Carbon 93, 59–67.

529 Zeng, L.X., Liu, R.P., Han, L., Luo, F.Q., Chen, X., Wang, J.B., Qian, Q.R., Chen, Q.H., Wei,
530 M.D., 2018. Preparation of a Si/SiO_2-ordered-mesoporous-carbon nanocomposite as an anode
531 for high-performance lithium-ion and sodium-ion batteries. Chem-Eur. J. 24, 4841–4848.
532 Zhang, W.S., Okutbayashi, S., Bechtold, T., 2005. Fibrillation tendency of cellulosic fibers-Part 4.
533 Effects of alkali pretreatment of various cellulosic fibers. Carbohyd. Polym. 61, 427–433.
534 Zhang, X., Hu, J.B., Chen, X.Y., Zhang, M., Huang, Q.Y., Du, X.Q., Liu, Y., Li, X.J., 2019.
535 Microtubular carbon fibers derived from bamboo and wood as sustainable anodes for lithium
536 and sodium ion batteries. J. Porous Mat. 26, 1821-1830.
537 Zhang, X., Huang, Q.Y., Zhang, M., Li, M.X., Hu, J.B., Yuan, G.M., 2020. Pine wood-derived
538 hollow carbon fibers@NiO@rGO hybrids as sustainable anodes for lithium-ion batteries. J.
539 Alloy. Compd. 822.
540 Zheng, P., Liu, T., Guo, S.W., 2016. Micro-nano structure hard carbon as a high performance anode
541 material for sodium-ion batteries. Sci. Rep-UK 6, 35620.